Application of a near-wall turbulence model to boundary layers and heat transfer

P. A. Durbin
Center for Turbulence Research, Stanford University, Stanford, CA, USA

A near-wall turbulence model based on k, ε, and $\overline{v^2}$ equations is described. It is used to predict flow and heat transfer in a two-dimensional channel and in boundary layers. Good agreement with data on skin friction, Stanton number, mean velocity, and turbulent intensities is obtained. Solutions to the model show the correct Reynolds number dependence without building it into any of the coefficients. Zero and adverse pressure gradient boundary layers are calculated; in both cases, the results agree well with experiment.

Keywords: turbulence model; boundary layer; convective heat transfer

Introduction

Heat and momentum transfer in turbulent boundary layers is controlled largely by a thin layer very near to the surface, within which turbulent mixing is suppressed by the proximity of the wall. The blocking effect of the solid boundary is manifested most clearly by the suppression of the normal component of turbulent intensity; precisely this component is responsible for transport to the boundary. It is shown in Durbin (1991), by using direct numerical simulation (DNS) data (Kim and Moin 1989), that near-wall "damping" of the eddy viscosity is caused by this suppression of the normal velocity; so if one uses the formula

$$\nu_t = C_\mu \overline{v^2} T \tag{1}$$

where T is a time scale and $\overline{v^2}$ is the variance of the normal component of turbulent velocity, then it is unnecessary to introduce ad hoc damping functions—as has been done in previous near-wall turbulence models. The essential requirement is a model to predict the behavior of the quantities in Equation 1 near to the wall. The k–ε–v model described herein was formulated for that purpose. This model should be viewed as a thin shear-layer approximation to a tensorally invariant Reynolds stress closure. It constitutes a necessary first step in the development of a model for more complex turbulent flows—the fact that the thin-layer model uses k, ε, and $\overline{v^2}$ as dependent variables should not confuse the main issue, which is exploration of the possibility of near-wall modeling by solving differential equations, rather than by ad hoc prescription of damping functions. In complex geometries the same approach to near-wall turbulence can be used in conjunction with a complete Reynolds-stress model (Durbin 1993).

The mathematical and physical basis of the present model is described in Durbin (1991). Essentially, kinematic blocking by the wall is introduced by an elliptic-relaxation equation for the redistribution terms in the Reynolds stress equations. That equation enables satisfaction of the boundary conditions; it also represents, in a somewhat indirect way, the nonlocal aspect of kinematic blocking. In the present paper, the equations of the model will be presented without repetition of the lengthy mathematical and physical rationalization that can be found in Durbin (1991). This is very much a follow-up to the previous paper, in which we assess the potential of the present approach by predicting boundary-layer flows: such assessment is an essential prerequisite to applying the approach to more complex flows.

Another unconventional feature of the present model is the "local anisotropy" term in the ε-equation, which was introduced in Durbin (1990). In calculations of turbulent channel flow, it was found that an enhanced production of ε was needed near the wall in order to obtain satisfactory agreement between model and data. It was proposed that this might be associated with linear production terms in the exact ε equation. These linear terms vanish if local isotropy (i.e., isotropy of the dissipation tensor) is satisfied. The apparent requirements of the modeling motivated a theoretical examination of the validity of the hypothesis of local isotropy (Durbin and Speziale 1991), with the conclusion that it was formally inconsistent with the Navier–Stokes equation when there was a significant mean rate of strain. This conclusion was cited in Durbin (1990) to justify an enhanced production of dissipation in the region of high mean shear, near to the surface—in practice, the modeling simply involves allowing C_{ε_1} to be a function of the ratio of kinetic energy production to dissipation.

Aside from these two innovations, the model is of a standard form. Its equations are the usual k–ε system and a common form of $\overline{v^2}$-equation, which is made into a fourth-order system of equations by coupling it to the previously cited elliptic equation for the redistribution term; this is referred to as the $\overline{v^2}$–f_{22} system of equations.

After briefly describing the model, we will show that the predictions of channel flow have not deteriorated (from Durbin 1991, 1990) by the present refinements to the model. Then we proceed to computations of momentum and heat transport in a flat-plate boundary layer. In addition to

Address reprint requests to Professor Durbin at the Center for Turbulence Research, Stanford University, Stanford, CA 94035-3030, USA.

Received 20 May 1992; accepted 23 February 1993

showing that the present model gives very good results for the zero pressure-gradient case, a computation is provided of the experiment by Samuel and Joubert (1974) on a boundary layer developing into an increasingly adverse pressure gradient. That experiment was undertaken specifically to provide data on a nonequilibrium boundary layer, against which turbulence models could be tested. It is shown in Rodi and Scheuerer (1976) that k–ε models with damping functions are unable to predict this flow. The present calculations are rather encouraging: good results were obtained without any adjustments to the model.

The model

The present model is similar to k–ε models: differential equations are solved for some components of the Reynolds stress, but the turbulent transport in the mean momentum equation is represented by an eddy viscosity. We consider boundary-layer flows, so Equation 1 is the only component of the eddy viscosity tensor that is needed. The essential difference between the present and the k–ε model is the use of an anisotropic eddy viscosity; indeed, the principal failure of the k–ε model near to boundaries, which ad hoc damping functions are required to correct, is that it is an isotropic model, while the near-wall turbulence is extremely anisotropic (Durbin 1990). Equation 1 is the 2-2-component of the anisotropic eddy-viscosity tensor (Launder 1989)

$$\nu_{t_{ij}} = C_\mu \overline{u_i u_j} T$$

The k–ε model uses the isotropic

$$\nu_{t_{ij}} = C_\mu \delta_{ij} k T$$

In the boundary-layer approximation, with the Reynolds shear stress replaced by an eddy viscosity, the steady mean momentum equation can be written

$$U\partial_x U = -\partial_x P + \partial_y((\nu + \nu_t)\partial_y U) \tag{2}$$

Equation 2 is expressed in von-Mises independent variables ($\Psi - x$)—that is, the partial derivatives with respect to x are at constant Ψ, and dy is understood to be $d\Psi/U$. The details of boundary-layer computation in these variables are well known (Patankar and Spalding 1970): a virtue of this formulation is that V is eliminated from the convective derivative. A boundary- layer code with an expanding mesh was written to solve Equation 2 and the turbulence model. The mesh was expanded by requiring that the 15th grid point from the top of the domain coincide with the 99 percent boundary-layer thickness. The eddy viscosity is given by Equation 1 in which

$$T = \max\left(\frac{k}{\varepsilon}, C_T\left(\frac{\nu}{\varepsilon}\right)\right) \tag{3}$$

This is just the usual time scale k/ε, with a lower bound by the Kolmogoroff scale. (The values of C_T and all other model constants are given in the nomenclature section.) Equation 3 introduces as viscous time scale near the surface. Equations that predict k, ε, and $\overline{v^2}$ are required to form a closed system.

The k–ε equations are standard (Rodi and Scheuerer 1986):

$$U\partial_x k = \mathscr{P} - \varepsilon + \partial_y\left(\left(\nu + \frac{\nu_t}{\sigma_k}\right)\partial_y k\right)$$

$$U\partial_x \varepsilon = \frac{C^*_{\varepsilon_1}\mathscr{P} - C_{\varepsilon_2}\varepsilon}{T} + \partial_y\left(\left(\nu + \frac{\nu_t}{\sigma_\varepsilon}\right)\partial_y \varepsilon\right) \tag{4}$$

in which $\mathscr{P}$ is the rate of energy production $\nu_t(\partial_y U)^2$. The only unconventional feature of Equations 4 is that $C^*_{\varepsilon_1}$ is allowed to be a function of $\mathscr{P}/\varepsilon$ to represent production by "local anisotropy." The linearized form

$$C^*_{\varepsilon_1} = C_{\varepsilon_1}(1 + a_1 \mathscr{P}/\varepsilon) \tag{5}$$

with $a_1 = 0.1$ was found adequate in Durbin (1990) and here; more generally, a non-linear dependence would be required to accommodate large values of $\mathscr{P}/\varepsilon$. Computations

Notation

Model constants

$C_\mu = 0.23$
$C_T = 6.0$

$k - \varepsilon$ system:

$a_1 = 0.1$
$C_{\varepsilon_1} = 1.44$
$C_{\varepsilon_2} = 1.9$
$\sigma_k = 0.9$
$\sigma_\varepsilon = 1.3$

$\overline{v^2} - \not{P}_{22}$ system:

$C_1 = 1.3$
$C_2 = 0.3$
$C_L = 0.2$
$C_\eta = 90$

Roman symbols

C_f	Friction coefficient, $2\tau_w/U_\infty^2$
C_{f_0}	Friction coefficient based on reference velocity in Samuel and Joubert (1974)
f_{22}	$\not{P}_{22}/k$
k	Kinetic energy
L	Length scale
$\mathscr{P}$	Rate of turbulent kinetic energy production
$\not{P}_{22}$	Velocity-pressure gradient correlation + term related to dissipation tensor
Pr	Prandtl number, ν/κ
R_τ	Reynolds-number-based friction velocity
R_θ	Reynolds number based on momentum thickness
St	Stanton number, $\kappa\partial_y\Theta(0)/U_\infty\Theta(\infty)$
T	Time scale
x, y	Horizontal and vertical coordinates
U, U_∞	Mean velocity and free-stream velocity
$u*$	Friction velocity, $\sqrt{\tau_w}$

Greek symbols

δ_{99}	Boundary-layer thickness of 99 percent
ε	Dissipation rate
θ	Boundary-layer momentum thickness
Θ	Mean temperature
κ	Diffusivity of temperature
ν	Viscosity
τ_w	Kinematic wall shear
Ψ	Stream function of mean flow

with $a_1 = 0$ produced inferior results, even after C_{ε_1} was increased to compensate for its omission. Thus, our experience is that this term is a clear improvement to the model. The present model addresses the near-wall problem and was calibrated using wall-bounded flows; Equation 5 may not give satisfactory spreading rates for free shear layers.

The boundary conditions to Equation 4 are that $k = \partial_y k = 0$ at no-slip boundaries. These two conditions on k suffice to determine the solution for the coupled system of equations (4); there is no need to impose conditions of ε at the wall—indeed, it would be incorrect to do so. The no-slip boundary condition guarantees the correct limiting behavior $k \to \varepsilon(0)y^2/2\nu$ as $y_+ \to 0$.

It is well known that boundary-layer calculations suffer from the difficulty that the turbulent energy goes to zero at the top of the layer, rather than having the physically correct y^{-4} fall off in the free stream. Here we follow the common expedient of introducing a small level of "free-stream turbulence" to avoid this difficulty. A level of 1 percent free-stream turbulence ($k = 10^{-4}U_\infty^2$) was used. However, the results were not sensitive to this, and were virtually identical with 0.1-percent free-stream turbulence: the essential properties of the model are determined by its near-wall behavior. The free-stream condition on ε is $\partial_y \varepsilon = 0$ at the top of the computational region.

The most important new aspect of the present model is its method of predicting $\overline{v^2}$. $\overline{v^2}$ is blocked by the boundary due to the no-normal-flux condition. Blocking is a kinematic effect; it is not associated directly with any term in the Reynolds stress dynamical equations. The boundary effect must be represented indirectly through the redistribution terms in the Reynolds stress balance (such as the pressure-strain). The boundary effect is associated with elliptic "action at a distance": that gives a rationale for introducing an elliptic relaxation model for the redistribution term. Also, the limiting behavior $\overline{v^2} \to O(y^4)$ as $y_+ \to 0$ cannot be met by Reynolds stress transport models; the elliptic relaxation model enables this boundary condition to be satisfied.

The $\overline{v^2}$-component of the Reynolds stress transport equation is

$$U\partial_x \overline{v^2} = \mathcal{f}_{22} - \overline{v^2}\frac{\varepsilon}{k} + \partial_y\left(\left(\nu + \frac{\nu_t}{\sigma_k}\right)\partial_y \overline{v^2}\right) \tag{6a}$$

Turbulent self-transport has been modeled by an eddy viscous term. $\mathcal{f}_{22}$ represents the unclosed redistribution term $-2\overline{v\partial_y p} - \varepsilon_{22} + \overline{v^2}\varepsilon/k$. The action at a distance of the wall is represented by an elliptic relaxation equation (Durbin 1991) for this term:

$$L^2\partial_y^2 f_{22} - f_{22} = (1 - C_1)\frac{\left[\frac{2}{3} - \overline{v^2}/k\right]}{T} - C_2\frac{\nu_t}{k}(\partial_y U)^2 \tag{6b}$$

in which

$$\mathcal{f}_{22} = kf_{22}$$

This last equation enforces the correct behavior $\mathcal{f}_{22} \to O(y^2)$ as $y_+ \to 0$. In the quasi-homogeneous limit, the model (6) reduces to the model of Launder et al. (1975). The elliptic relaxation equation contains a length scale L that describes spatial decorrelation of turbulent eddies and a Laplacian to account for geometrical fall-off of correlations. The Laplacian can be considered a consequence of the Laplacian in the Poisson equation for pressure. In general the elliptic relaxation equation introduces kinematics into near-wall turbulence models; these kinematics might be associated with blocking or with pressure reflection (Launder et al. 1975).

The length scale in Equation 6b is prescribed as

$$L = C_L \max\left(\frac{k^{3/2}}{\varepsilon}, C_\eta\left(\frac{\nu^3}{\varepsilon}\right)^{1/4}\right) \tag{7}$$

by analogy to Equation 3.

At a no-slip boundary, the correct behavior of $\overline{v^2}$ is $\overline{v^2} = O(y^4)$. The model is formulated such that this condition can be met: the general solution to Equation 6a as $y \to 0$ is

$$\overline{v^2} \to Ay^2 + \frac{B}{y} + \varepsilon(0)f_{22}(0)\frac{y^4}{20\nu^2}$$

where A and B are integration constants. The boundary condition amounts to requiring that $A = B = 0$. In practice the $\overline{v^2} - \mathcal{f}_{22}$ equations were solved as a coupled system using a block tridiagonal solver, with the limiting condition $\overline{v^2} \to \varepsilon(0)f_{22}(0)y^4/20\nu^2$ imposed. The subroutine to solve this system was the same as that used to solve the coupled k–ε system, with the limiting condition $k \to \varepsilon(0)y^2/2\nu$ imposed. In the free stream $\partial_y \mathcal{f}_{22} = 0$, and the isotropy condition $\overline{v^2} = 2k/3$ are prescribed.

The feasibility of the present model was originally demonstrated by making use solely of DNS channel flow data (Durbin 1991). Model constants could be set fairly coarsely for that purpose. In the boundary layer, the need to predict the growth rate of the momentum thickness requires more refined values of the constants. An attempt has also been made to bring the constants into line with values used by other modelers: for example, previously the round numbers $C_{\varepsilon_1} = 1.5$ and $C_{\varepsilon_2} = 2.0$ were found adequate for the initial formulation of the model; they have now been set to the more conventional values $C_{\varepsilon_1} = 1.44$ and $C_{\varepsilon_2} = 1.9$. Various other refinements are reflected by the values in the nomenclature section.

Heat transfer was computed by solving

$$U\partial_x \Theta = \partial_y\left(\left(\kappa + \frac{\nu_t}{\mathrm{Pr}_t}\right)\partial_y \Theta\right) + Q \tag{8}$$

which is analogous to Equation 2—von-Mises variables are used again. Turbulent transport of heat is modeled by an eddy diffusivity equal to ν_t/Pr_t, where Pr_t is the turbulent Prandtl number. The source term Q was zero in the boundary-layer computations. It is included in Equation 8 for the channel flow computations described next.

Channel flow

In fully developed channel flow, the x-derivatives in the momentum, temperature, and model equations are identically zero. Hence, this case reduces to the solution of ordinary differential equations. Such computations are described at length in Durbin (1991). For the present study, the channel flow was recomputed to verify that the agreement with data was not deteriorated by the present refinements to the model constants. Figure 1 is a comparison between the present model and DNS channel flow data at $R_\tau = 395$: Figure 1a is a linear plot and Figure 1b (added upon the request of reviewers) is a log-linear plot to show the wall region in more detail. The agreement between model and data is satisfactory. A similar level of agreement was obtained between the model and DNS data at $R_\tau = 180$; in the interest of brevity, that computation is not shown. Almost perfect agreement would be obtained if the values of $\sigma_k = 1.3$

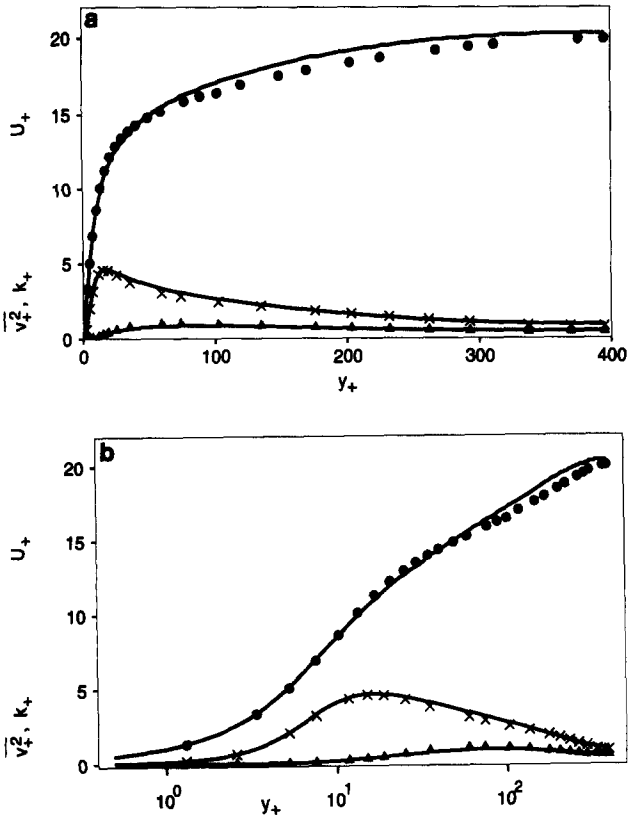

Figure 1 Comparison of model (—) to DNS (symbols) data for channel flow at $R_\tau = 395$. ●, U; ×, k; ▲, $\overline{v^2}$. (a) Linear-linear, (b) log-linear

and $\sigma_\varepsilon = 1.6$ were used; these are the values found in Durbin (1991) when the model was calibrated solely using low Reynolds number DNS channel flow data. It is clear that no universal model constants exist; the calibration process involves compromise within a range of flows.

Temperature profiles were found by solving Equation 8 numerically. In Kim and Moin (1989), the source Q was a constant and the boundary conditions were $\Theta = 0$ at the walls. These are the conditions imposed on the solutions in Figure 2. This figure shows mean temperature profiles for molecular Prandtl numbers of 2.0, 0.71, and 0.1 compared to DNS data: the agreement is quite good. For the solid curves, the turbulent Prandtl is 0.9, which is representative of the values found by Kim and Moin (1989) in the near-wall region when Pr = 2.0 or 0.71; when Pr = 0.1, higher values (around 1.4) were observed, but no allowance for the turbulent Prandtl number to depend on molecular Prandtl number has been made in the computations shown by solid lines. For this reason the good agreement between data and model at Pr = 0.1 may be fortuitous—it probably is a peculiarity of the fact that the Peclet number, Pr × R_τ, is very low. The dashed curves in Figure 2 were computed with Equation 9 and are shown for consistency with later boundary-layer computations. In this case, the turbulent Prandtl number is a function of turbulent Peclet number. The two Prandtl number prescriptions show similar levels of agreements with the data.

Boundary-layer computations

Channel flow calculations were described in the last section to show that the present revisions to the model constants did not deteriorate previous results. The main purpose of this paper is to present new model computations for boundary-layer flow and heat transfer, thereby assessing the potential of our proposed approach to modeling near-wall turbulence. The model equations were solved initially for the zero pressure gradient flat-plate boundary layer. The computations were initialized by interpolating DNS data provided by Spalart (1988); the data at $R_\theta = 670$ were used. There was a rapid initial transient during which the profiles were adjusted by the model equations because these data are not an equilibrium solution to our closure model. After that transient, the solution evolved downstream more slowly and became largely insensitive to initial conditions.

Figure 3 shows the skin-friction coefficient versus momentum thickness Reynolds number, compared to various experimental data: the agreement is quite encouraging. The Weighardt and Tillman data (Coles and Hirst 1968) cover the widest range of R_θ, and have been reproduced by others in many subsequent experiments. There is a noticeable discrepancy between model and data at the lowest R_θ shown. However, at these Reynolds numbers, experimental boundary layers are sensitive to how they are tripped (Purtell et al. 1981), and in unforced flow they would be transitional. Quantitative discrepancies here are not surprising; qualitatively, the tendency of C_f to rise steeply at low Reynolds number is reproduced by the model.

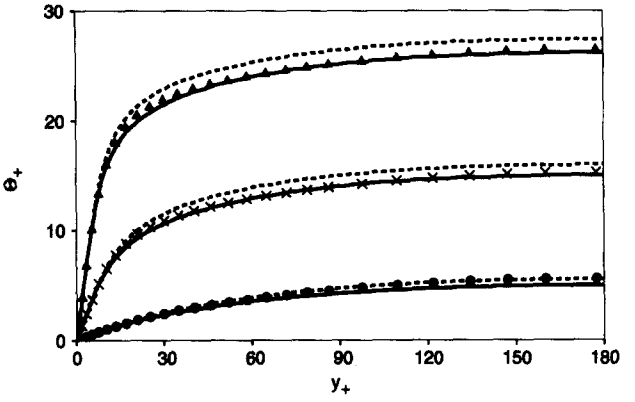

Figure 2 Mean temperature profiles compared to DNS data at various molecular Prandtl numbers and $R_\tau = 180$. ●, Pr = 0.1; ×, Pr = 0.71; ▲, Pr = 2.0. —, $Pr_t = 0.9$; - - -, Pr_t given by Equation 9

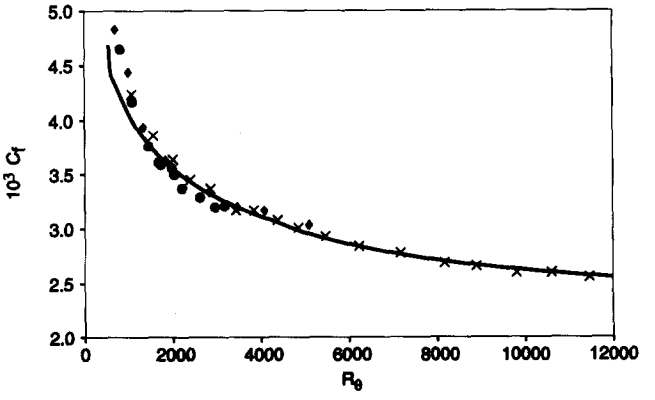

Figure 3 Friction coefficient versus momentum thickness Reynolds number in zero pressure-gradient boundary layer. Experimental data: ×, Weighardt and Tillman (Coles and Hirst 1968); ●, Bell (Coles and Hirst 1968); ◆, Purtell et al. (1981)

In Figure 4 mean velocity profiles at various R_θ between 1,400 and 11,000 are compared to experimental data tabulated in Coles and Hirst (1968). Variables are in wall units ($y_+ = yu_*/\nu$ and $U_+ = U/u_*$). Although the lower Reynolds number profiles are somewhat compacted, expanded plots show that they agree with the experimental data as well as do the higher Reynolds number cases. Hence, the model is reproducing the Reynolds number dependence displayed by the data *without* any Reynolds number dependence of the model constants; the exact viscous terms in Equations 2, 4, and 6 seem to adequately represent Reynolds number effects.

An even more detailed assessment of the model is provided by Figure 5. This shows a comparison of turbulence statistics to data transcribed from Klebanoff (1955); R_θ is 7,150. The computed kinetic energy shows a sharp peak near the wall, as do the data, although some quantitative discrepancy exists. In the outermost portion of the boundary layer, the experimental data fall off a bit more rapidly than the computation. The solution for the normal component of intensity is in quite good accord with the data; this is important because the $\overline{v^2}$-component is responsible for turbulent transport toward the wall.

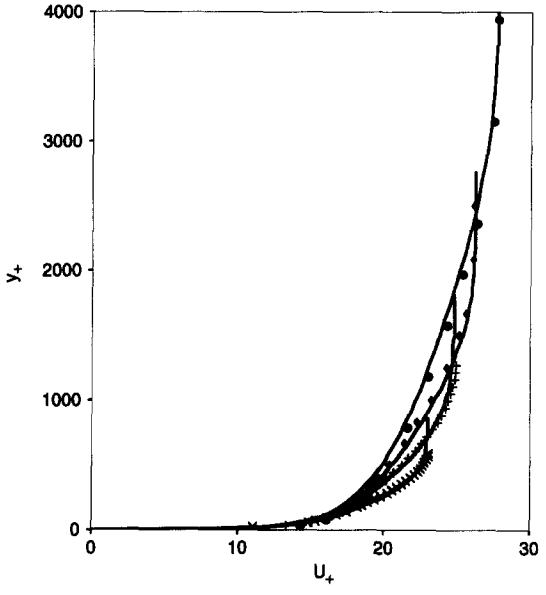

Figure 4 Mean velocity profiles in zero pressure-gradient boundary layer at $R_\theta = 1451$ (×), 3195 (+), 5473 (◆), and 10611 (●)

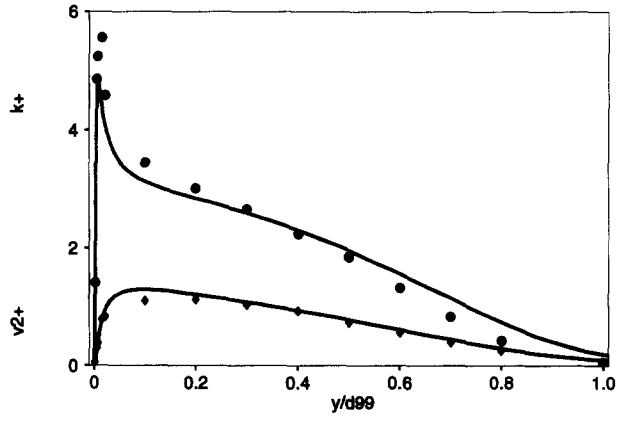

Figure 5 Profiles of k (●) and $\overline{v^2}$(◆) at $R_\theta = 7{,}150$ in a zero pressure-gradient boundary layer. Experimental data were transcribed from Klebanoff (1955)

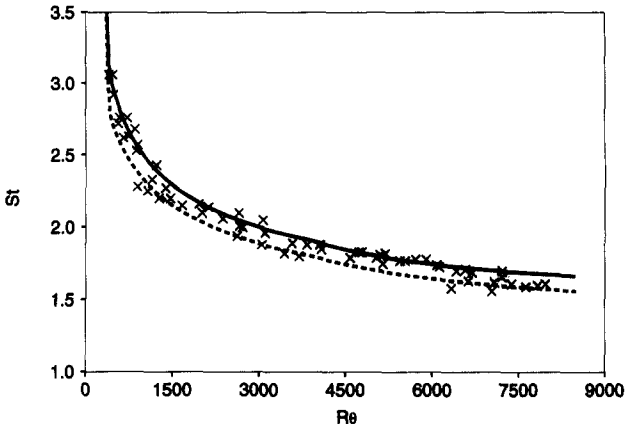

Figure 6 Stanton number versus momentum thickness Reynolds number is zero pressure-gradient boundary layer. Data from Reynolds et al. (1958). —, $Pr_t = 0.9$; - - -, Equation 9

Heat transfer coefficients in the form of Stanton number versus momentum thickness Reynolds number are portrayed by Figure 6. They are compared to experimental data from Reynolds et al. (1958); Moffatt and Kays (1984) describe these data as representative of those measured in many subsequent experiments. The molecular Prandtl number is 0.71, corresponding to air. Two computations are shown in the figure: one was done with $Pr_t = 0.9$ and is shown by the solid curve; the other was done with PR_t given by the formula

$$Pr_t = \frac{1.7}{1 + 0.4Pe_t + 0.08(e^{-5/Pe_t} - 1)Pe_t^2} \tag{9}$$

and is shown by the dashed curve. In Equation 9, Pe_t is the turbulent Peclet number ν_t/κ. Equation 9 is the Prandtl number–Peclet number relation given by Moffatt and Kays (1984), and 0.9 is the value they recommend if a constant Prandtl number is to be used instead. Equation 9 has the property of rising steeply near the wall, reaching 1.7 at $y = 0$, and tends to 0.85 far from the wall. A steep rise of Pr_t is seen experimentally when $y_+ < 15$ (Moffatt and Kays 1984). Both of the curves in Figure 6 are within the data scatter: the constant Prandtl number curve (solid) would seem to be in slightly better agreement, although the two curves are within 10 percent of each other.

Figure 7 shows a more stringent test of the near-wall behavior of the turbulent transport model. The upper curve and ×'s are a computation and data from Reynolds et al. (1958) of heat transfer in a boundary layer with a step in temperature at $R_\theta = 2{,}280$. Upstream the plate is unheated; hence, in the downstream, heated region the thermal boundary layer develops into a pre-existing flow boundary layer. Transport processes very near to the wall then determine the dynamic response of the Stanton number to this abrupt change in boundary condition. In the computation the wall temperature was raised from 0 to 1 in a single downstream step. This caused the Stanton number to become extremely large at the start of the heating; of course, in the experiment such a sharp step was impossible. Data and a computation for a uniformly heated plate (+) are included in Figure 7. One sees that the rate of relaxation toward the uniformly heated St vs. R_θ curve is predicted quite well by the model. The model lies a bit above the data, due to the differences in initial conditions, but parallel to it, showing that the model has the right dynamical behavior.

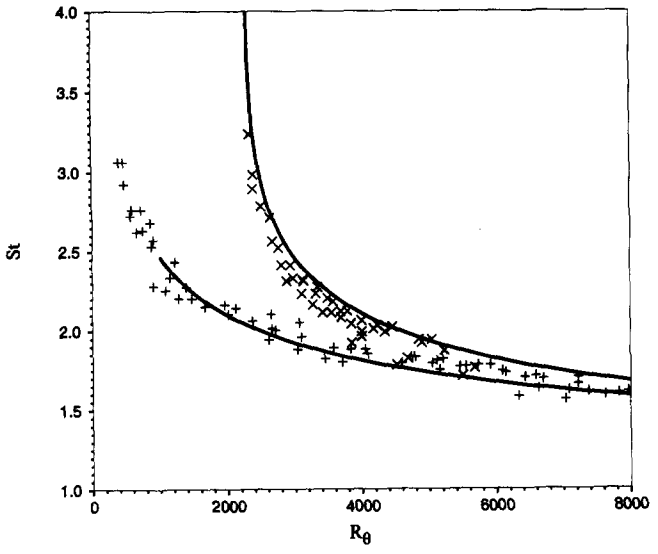

Figure 7 Stanton number versus momentum thickness Reynolds number for Reynolds et al. (1958) experiment with step heating. (×) Step in wall temperature at $R_\theta = 2{,}280$; (+) uniformly heated wall

By an R_θ of about 5,500, the experimental data for the step and uniform heating have mingled. The model predicts the two cases to approach asymptotically as $R_\theta \to \infty$, as might be expected.

Mean temperature profiles for the case of a uniformly heated plate are compared to data of Reynolds et al. (1958) in Figure 8 at two values of R_θ. A clear discrepancy exists between the model and data: although the model profiles have the right shape and the correct gradient near the wall, they fall above the data in the center of the boundary layer. Equation 9 was intended to improve the agreement between model and experimental temperature profiles. At the higher Reynolds number, it does produce an improvement. Ultimately, it would seem more in keeping with the spirit of Reynolds stress closure modeling to develop an eddy heat-flux equation rather than use an explicit Pr_t–Pe_t relationship; for the time being Equation 9 seems an adequate stop gap.

It is hoped that the physical and mathematical basis of the present model will make it more flexible than k–ε models, with damping functions to correct their near-wall behavior. The next three figures are in this vein.

Samuel and Joubert (1974) reported an experiment on a boundary layer developing into an increasingly adverse pressure gradient. Motivated by the Stanford boundary-layer conference (Coles and Hirst 1968), they set up a simple non-equilibrium flat-plate flow against which models can be tested. Rodi and Scheuerer (1986) found than a k–ε model with eddy-viscosity damping considerably overpredicted the skin-friction data. Hence, this is a useful experiment for testing how a turbulence model fares in nonequilibrium flow. Rodi and Scheuerer added an extra production term to their ε-equation, with an adjustable constant, solely to fit a computation to Samuel and Joubert's data. As Rodi and Scheuerer noted, the extra term has an inappropriately large coefficient and violates the principle of tensorial invariance.

An initial condition for the present computation was obtained by starting with a zero pressure-gradient boundary layer slightly upstream of the first measurement location, then subjecting it to the initial pressure gradient reported by Samuel and Joubert (1974). The upstream distance at which the pressure gradient was imposed was determined as follows: at the first measurement location $R_\theta = 4{,}992$, while $C_f = 2.79 \times 10^{-3}$; a zero pressure-gradient boundary layer at this R_θ would have $C_f = 3.0 \times 10^{-3}$. It was found that the correct initial friction coefficient could be obtained by applying the pressure gradient to a zero pressure-gradient boundary layer with $R_\theta = 3{,}200$ and allowing it to develop downstream to the position where $R_\theta = 4{,}992$, so this is how the computation was initialized. The shape of the initial mean velocity profile is very close to the zero pressure-gradient form, as are the k and $\overline{v^2}$ profiles; hence, our initialization procedure is analogous to starting with measured profiles, but preferable because it also provides initial conditions for ε and f_{22}.

The pressure gradient versus downstream distance tabulated in Table 1 of Samuel and Joubert (1974) was imposed on the present model. The resulting downstream evolution of friction coefficient and displacement thickness are shown in Figure 9. The agreement is rather good. No alterations to the model used in the previous zero pressure-gradient and channel flow computations were made. Thus, one sees that the extra production term added by Rodi and Scheuerer to the k–ε model to bring it closer to the data is not required; also, this term is not consistent with the boundary-layer approximation, so ought not be added.

The abscissa in Figure 9 is downstream distance in meters because this is how Samuel and Joubert (1974) report their data—note that we have set the origin of x at the first measurement station. For the computations, the reported value of unit Reynolds number $d\,\mathrm{Re}/dx = 1.7 \times 10^6\ \mathrm{m}^{-1}$ was used to nondimensionalize both distance and the C_p gradient reported in their Table 1. Samuel and Joubert also define C_f as the friction coefficient based on the upstream reference velocity; this is how the computations are normalized in Figure 9.

The present model also shows agreement with data on the evolution of the k and $\overline{v^2}$ profiles. Figure 10 shows computed kinetic energy and $\overline{v^2}$ profiles at three downstream locations. They are normalized by the upstream reference velocity. Figure 10 makes it clear that this is a significantly nonequilibrium flow. It often seems that the near-wall portion of *mean flow* profiles can be collapsed to their zero pressure-gradient form

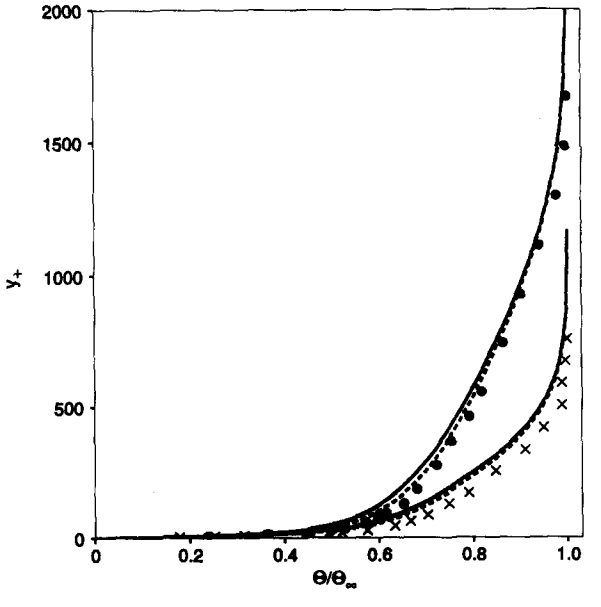

Figure 8 Temperature profiles at $R_\theta = 1763$ (×) and 4432 (●). Lines are as in Figure 6

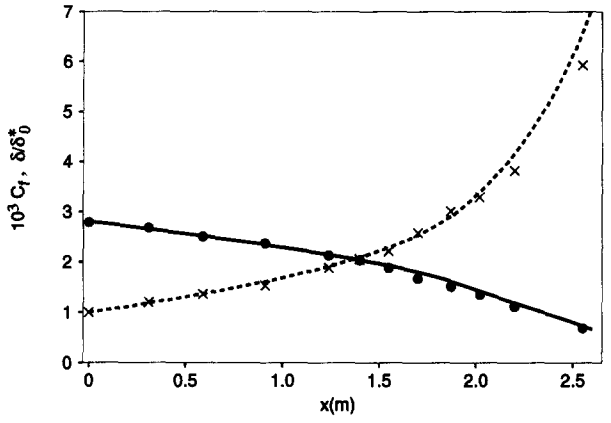

Figure 9 Friction coefficient (●) and displacement thickness (×) versus downstream distance for the Samuel and Joubert adverse pressure-gradient boundary layer

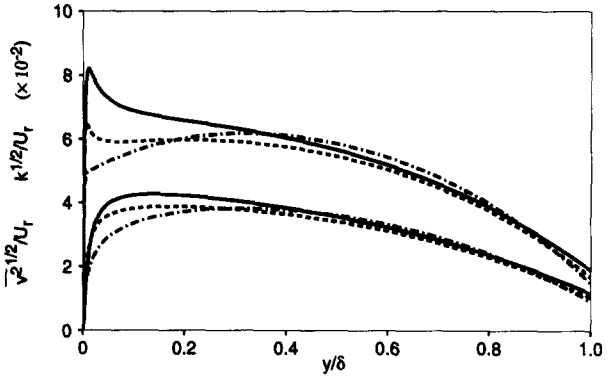

Figure 10 Turbulent intensities for the Samuel and Joubert experiment at $x = 0.1$ m (—), 1.87 m (- - -), and 2.55 m (—·—)

by plotting in wall units; in particular, log-linear plots seem often to have a linear portion with the same slope and intercept as in zero pressure-gradient flow—even though the pressure gradient is far from zero. In light of Figure 10 and similar results in Samuel and Joubert (1974), this collapse of the mean flow is rather puzzling. *Turbulence statistics*, including the Reynolds shear stress, show significant departures from equilibrium in flows for which the wall region is described as being in "equilibrium" on the basis of wall unit plots of the mean velocity profile.

Figure 10 can be compared to Figure 16 of Samuel and Joubert (1974): the experiments also show the movement of the peak kinetic energy toward the wall, with it disappearing at the last measurement station, and the increasing suppression of $\overline{v^2}$ near the surface. The predicted magnitudes of $k^{1/2}/U_\tau$ and $\overline{v^2}^{1/2}/U_\tau$ also are in rough accord with the data. The primary point of disagreement is the behavior in the outermost part of the boundary layer: here the data show k and $\overline{v^2}$ to be largest at $x = 2.55$ m, while they are smallest in the model computation. This possibly is a result of outer region intermittency not being suitably represented by the model. The outer region only has a weak effect on the mean velocity and skin friction.

In Figure 11, mean flow profiles are displayed at $x = 1.87$ m and 2.55 m along with experimental measurements. The agreement at 1.87 m is rather good. At the station farthest downstream, U/U_∞ has risen to about 0.3 at the top of the region of steep gradient (the viscous sublayer) next to the surface; in the experiments, this quantity rises to about 0.36. Consequently, the wake deficit is overpredicted by the model at this location.

One might ask why the present model performs better than the k–ε–damping-function model in adverse pressure-gradient flow. An explanation follows from Figures 5 and 10: the k–ε model replaces the velocity scale $\overline{v^2}$ in Equation 1 by k, thereby making the eddy viscosity isotropic. The "damping function" that then is needed to fit the model to data is a correction for the lack of anisotropy in the model and its presence in the flow—this explanation of the nature of the eddy-viscosity damping function was also given by Launder (1986). Comparing the k and $\overline{v^2}$ profiles in Figure 5, one sees that in order to mirror the $\overline{v^2}$ profile, the k profile must be multiplied by a function of y_+ that suppresses its near-surface peak. This damping function of y_+ is fixed once and for all; hence, it is unable to respond to dramatic changes of the turbulence profiles, like those occurring downstream in Figure 10. It is clear that the damping function is peculiar to a given flow—and this probably is why a plethora of functions have been used by various modelers. In a strong pressure gradient, the sharp peak of k near the wall is suppressed as the maximum rate of energy production moves away from the surface; the fixed damping function is unable to reflect these changes. The present model is formulated in terms of turbulence statistics alone, and profiles of these statistics are found by solving differential equations; the objective in doing so is to allow them to respond to conditions of the flow.

Previous investigators (Rodi and Scheuerer 1986) have proposed that the failure of the k–ε–damping-function model in both equilibrium and nonequilibrium adverse pressure-gradient flow was due to shortcomings in the ε equation, their reasoning being that the length scale of the turbulence was incorrectly determined by ε. The practice of using ε to determine a length scale has serious faults; however, the present results suggest that the difficulties experienced by the k–ε model in adverse pressure gradients is primarily a consequence of using k for the velocity scale; the ε equation seems to perform satisfactorily.

As a last assessment of the model, plane Couette flow has been computed. Experiments on this flow are described by El Telbany and Reynolds (1982); a DNS was performed by Lee (1990). This case was included in the present paper on the advice of a reviewer. However, it should be noted that Lee found the turbulence to be dominated by large-scale,

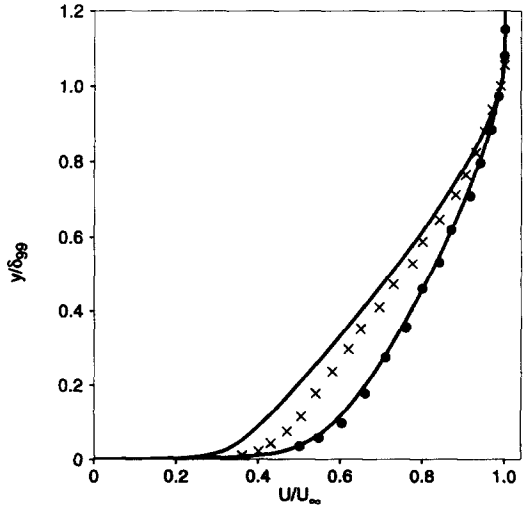

Figure 11 Mean velocity profiles at $x = 1.87$ m (●) and 2.55 m (×) of the Samuel and Joubert experiment

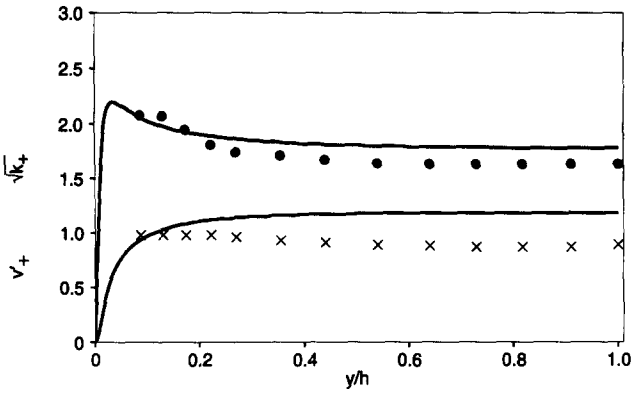

Figure 12 Profiles of $\sqrt{k_+}$(●) and v'_+(×) at $R_\theta = 10^4$ in plane Couette flow. Experimental data were transcribed from El Telbany and Reynolds (1982)

quasi-steady, streamwise eddies; these eddies do not form in similar Poiseulle flow and boundary-layer simulations. He advised that this was not a representative case against which to test models (private communication). Gibson (1988) also noted certain peculiarities of plane Couette flow that make it unlike other plane shear layers. He hypothesized that counter-gradient transport of turbulent energy might occur near the center of the channel.

Figure 12 shows a comparison of model solutions and data of El Telbany and Reynolds (1982) on $v'/u*$ and $\sqrt{k}/u*$. These are at a Reynolds number $U_{wall}h/\nu = 10^4$, where h is the half-height of the channel. The general features are that k has a peak near the wall and both k and $\overline{v^2}$ are constant in the central portion of the channel. The model and data agree on this, although the model overpredicts the levels of the turbulent intensities. Similarly, the model overpredicts the skin-friction coefficient measured by El Telbany and Reynolds by about 16 percent; thus it is at the upper end of the data scatter in Figure 5 of El Telbany and Reynolds (1982). Our results agree with Gibson's (1988) conclusion that models that work well in other wall-bounded shear flows tend to be more inaccurate in plane Couette flow.

Conclusions

The focus of the present paper was the refinement and assessment of an approach to near-wall closure modeling suggested in Durbin (1991). In that approach, equations come in coupled pairs—k–ε and $\overline{v^2}$–f_{22}; this enables boundary conditions to be satisfied and an elliptic wall blocking effect to be introduced. $\overline{v^2}$ is the appropriate velocity scale for the eddy viscosity near a solid boundary. In the cases discussed here, k/ε seems to be an appropriate time scale. In more rapidly evolving flows, one would expect this time scale to be inappropriate; the eddy-viscosity approximation for the Reynolds shear stress would also be unjustified.

A model for wall-bounded thin shear layers was presented and assessed by comparing numerical solutions for mean flow, turbulence statistics, and heat transfer to experimental and DNS data. The model is currently being used to compute a pressure-driven separation bubble; it is not limited in its applicability to attached flow. However, its simple form would be inappropriate to complex geometries in which the $\overline{v^2}$ component cannot be singled out. If the flow contained massive separation, a model calibrated using wall-bounded shear flow data could be expected to be inaccurate.

Acknowledgement

I am grateful to Dr. J. Kim for reviewing the manuscript.

References

Coles, D. E. and Hirst, E. A. 1968. *Computation of Turbulent Boundary Layers.* AFOSR–IFP–Stanford Conference, Stanford University

Durbin, P. A. 1991. Near-wall turbulence closure modeling without 'damping functions.' *Theoret. Comput. Fluid Dynamics*, **3**, 1–13

Durbin, P. A. 1993. A Reynolds stress model for near-wall turbulence. *J. Fluid Mech.*, **249**, 465–498

Durbin, P. A. 1990. Turbulence closure modeling near rigid boundaries. Center for Turbulence Research Annual Research Briefs, Stanford University

Durbin, P. A. and Speziale, C. G. 1991. Local anisotropy in strained turbulence at high Reynolds numbers. *ASME J. Fluids Eng.*, **113**, 707–709

El Telbany, M. M. and Reynolds, A. J. 1982. The structure of turbulent plane Couette flow. *J. Fluids Eng.*, **104**, 367–372

Gibson, M. M. 1988. Analysis of turbulent Couette flow with a Reynolds stress model. Imperial College MED Report FS/88/54, London

Kim, J. and Moin, P. 1989. Transport of passive scalars in a turbulent channel flow. *Turbulent Shear Flows*, **6**, 85–95

Klebanoff, S. 1955. Characteristics of turbulence in a boundary layer with zero pressure gradient. NACA Report, **1247**

Launder, B. E. 1989. Second-moment closure: present... and future. *Int. J. Heat Fluid Flow*, **10**, 282–300

Launder, B. E. 1986. Low Reynolds number turbulence near walls. Report TFD/86/4, Mechanical Engineering Department, UMIST, Manchester, UK

Launder, B. E. Reece, G. J., and Rodi, W. 1975. Progress in the development of Reynolds stress turbulence closure. *J. Fluid Mech.*, **68**, 537–566

Lee, M. J. 1990. The large scale structures in turbulent plane Couette flow. Center for Turbulence Research Annual Research Briefs, Stanford University

Moffatt, R. J. and Kays, W. M. 1984. A review of turbulent boundary layer heat transfer research at Stanford 1958–1983. *Adv. Heat Transf.*, **16**, 241–365

Patankar, S. V. and Spalding, D. B. 1970. *Heat and Mass Transfer in Boundary Layers*, 2nd ed. Intertext, London

Purtell, L. P., Klebanoff, S., and Buckley, F. T. 1981. Turbulent boundary layer at low Reynolds number. *Phys. Fluids*, **24**, 802–811

Reynolds, W. C., Kays, W. M. and Kline, S. J. 1958. Heat transfer in the turbulent incompressible boundary layer. NACA memo. **12-1- 58w**

Rodi, W. and Scheuerer, G. 1986. Scrutinizing the k–ε model under adverse pressure gradient conditions. *ASME J. Fluids Eng.*, **108**, 174–180

Samuel, A. E. and Joubert, P. N. 1974. A boundary layer developing in an increasingly adverse pressure gradient. *J. Fluid Mech.*, **66**, 481–505

Spalart, P. 1988. Direct simulation of a turbulent boundary layer up to $R_\theta = 1400$. *J. Fluid Mech.*, **187**, 61–98